DISCRETE AND CONTINUOUS
DYNAMICAL SYSTEMS SERIES B
Volume , Number **0**, pp. **000–000**

ON THE STABILITY OF THE LAGRANGIAN HOMOGRAPHIC SOLUTIONS IN A CURVED THREE-BODY PROBLEM ON $\mathbb{S}^2$

Regina Martínez

Departament de Matemàtiques
Universitat Autònoma de Barcelona
Bellaterra, Barcelona, Spain

Carles Simó

Departament de Matemàtica Aplicada i Anàlisi
Universitat de Barcelona
Gran Via 585, 08007 Barcelona, Spain

(Communicated by)

Abstract. The problem of three bodies with equal masses in $\mathbb{S}^2$ is known to have Lagrangian homographic orbits. We study the linear stability and also a "practical" (or effective) stability of these orbits on the unit sphere.

A nuestro buen amigo Ernesto Lacomba,
en recuerdo de años pasados y con
nuestros mejores deseos para los venideros.

1. **Introduction.** The classical (Euclidean) N-body problem in $\mathbb{R}^2$ or $\mathbb{R}^3$ was modified by Bolyai and Lobachevsky near 200 years ago to consider the case of curved spaces. Since then it has received sporadically some attention, but the interest has been renewed in the last years with several contributions. We refer to the nice paper [1] for historical details and basic results. In particular that paper proves the existence of several kinds of Lagrangian-like homographic orbits and classifies all the possible solutions of this type. In [1] both the Lagrangian and Eulerian homographic solutions are studied and the curvature κ is kept as a parameter.

As in the classical case one can scale the masses of the three bodies so that the sum of the masses is equal to 1 or, if the masses are equal, they can be all set to 1. But the curvature κ cannot be scaled. Hence, it is an essential parameter in the problem. But in what follows we shall consider just the motion on the sphere of radius 1. The methodology used in present paper can be extended to arbitrary positive values of κ, but the results will be different.

Our main point is that not only the existence of periodic solutions (either in a fixed or rotating frame) is relevant, but mainly its local stability properties. Another question that we face is that even orbits starting close to unstable homographic

2000 *Mathematics Subject Classification.* Primary: ; Secondary: .
Key words and phrases. curved 3-body problem, stability of solutions, homographic orbits, practical stability.

solutions can move, during a very long time, in a vicinity of moderate size of these orbits due to the existence of many invariant nearby tori and its sticky properties.

We consider the motion of three point particles of masses equal to 1 moving on $\mathbb{S}^2$ embedded in $\mathbb{R}^3$. Let $\mathbf{q}_i, i = 1, 2, 3$ denote the position of the i-th mass. Hence, if we denote as $(\ ,\ )$ the scalar product, we have $(\mathbf{q}_i, \mathbf{q}_i) = 1$. The force function which extends from the plane to $\mathbb{S}^2$ is

$$U(\mathbf{q}) = \sum_{1\le i<j\le 3} \frac{(\mathbf{q}_i, \mathbf{q}_j)}{[1-(\mathbf{q}_i, \mathbf{q}_j)^2]^{1/2}}.$$

The equations of motion are a particular case of the equations (8) in [1] and read as

$$\ddot{\mathbf{q}}_i = \sum_{j=1, j\neq i}^{3} \frac{\mathbf{q}_j - (\mathbf{q}_i, \mathbf{q}_j)\mathbf{q}_i}{[1-(\mathbf{q}_i, \mathbf{q}_j)^2]^{3/2}} - (\dot{\mathbf{q}}_i, \dot{\mathbf{q}}_i)\mathbf{q}_i, \quad i = 1, 2, 3, \tag{1}$$

where $\dot{}$ denotes differentiation with respect to the time t. In contrast with the Euclidean case that system no longer has the centre of mass integrals, but it keeps the energy and angular momentum integrals. Concretely if $T = \frac{1}{2}\sum_{i=1}^{3}(\dot{\mathbf{q}}_i, \dot{\mathbf{q}}_i)$ and $H = T - U$ and $\mathbf{c} = \sum_{i=1}^{3} \mathbf{q}_i \wedge \dot{\mathbf{q}}_i$ then H and $\mathbf{c}$ are first integrals. Due to the invariance of the equations in (1) under the action of $SO(3)$ one can always assume that $\mathbf{c}$ points in the direction of the positive z axis if $\mathbf{c} \neq 0$. The modulus of $\mathbf{c}$ will be denoted simply as c.

A Lagrangian-like solution is a solution of (1) in which the three masses form an equilateral triangle for all t. In [1] it is proved (Theorem 4) that these solutions are only possible with three equal masses. This is why we restrict our attention to this case. Furthermore the possible Lagrangian-like solutions, in any sphere of arbitrary radius, belong to different classes, as given by Theorem 2 in [1]. We present these results in a slightly modified version, adapted to the unit sphere. This will be obtained from the phase portrait of the Hamiltonian $\mathcal{H}_z$ to be introduced in Section 3 (see Figure 3). So, the Lagrangian-like solutions belong to one of the following types.

1) If $c = 0$ then there are
   a) Fixed points at the equator.
   b) Homothetic orbits, analogous to the homothetic orbits in the planar case, which are ejected from the north pole and return to collision with the north pole after reaching a minimal value z_m of z which is positive. Each one of the masses moves along a meridian. Symmetrical orbits exist exchanging north pole by south pole and being now z_m, negative, the maximal value of z.
   c) Homothetic orbits ejected from the north pole and going to collision at the south pole and vice versa.
   d) Finally we find orbits ejected from the north pole and going asymptotically to the equator when $t \to +\infty$. They spiral towards the equator. Also the orbits symmetrical of these one by time reversal and the corresponding ones in the southern hemisphere.
2) If $0 < c^2 < 8/\sqrt{3}$ then there are
   a) A relative equilibrium solution with the bodies at the equator,
   b) Relative equilibrium solutions, with the bodies moving in a parallel, which depends on the modulus of $\mathbf{c}$ with constant angular velocity. Thet can be seen as fixed points in a rotating frame. It is analogous to the planar

case. There are two such solutions, one in the northern and one in the southern hemisphere.

c) Homographic solutions, such that the bodies rotate with non-constant angular velocity and the distance between them is changing. There are three kinds of these orbits: the ones confined to the northern hemisphere with $0 < z_{\min} < z < z_{\max} < 1$, the symmetrical ones confined to the southern hemisphere, and the orbits which visit, in a symmetric way, both hemispheres crossing the equator and ranging in $-1 < -z_{\max} < z < z_{\max} < 1$.

d) Finally there are "separatrix" like orbits, either in one hemisphere or the other, which reach an extreme value of z, depending on the modulus of $\mathbf{c}$, and go spiraling asymptotically to the equator for $t \to \pm\infty$, approaching the relative equilibrium solution at the equator (with some phase shift).

3) If $c^2 \geq 8/\sqrt{3}$, only the relative equilibrium at the equator, like in 2a), and the homographic solutions which cross the equator like in 2c), subsist.

Full details and some illustrations will be given in Section 3.

We shall study the case 2b) and the homographic solutions confined to the northern hemisphere of the case 2c). We have found relevant differences with the planar case.

For the relative equilibrium solutions in the planar three-body problem, according to the classical results (see e.g. [7]), the Siegel exponents for these solutions give instability. For the relative equilibria in 2b) of the three-body problem in $\mathbb{S}^2$, we show that there are ranges of the angular momentum for which these orbits are linearly stable. This is the contents of Section 2.

In the homographic case 2c) a first difference with the planar problem is that the orbits are quasiperiodic in a fixed frame (unless the ratio of the frequencies is rational, which is a zero measure case), while in the planar case they are periodic, with the three bodies moving in ellipses. Furthermore, results in [5] (already announced in [4]) show that the Lagrangian-like homographic orbits for equal masses are totally hyperbolic. In the present case there are open sets of energy and momentum for which these orbits are stable. These properties are studied in Sections 3 and 4.

Finally Section 5 is devoted to study the dynamics of homographic orbits by direct numerical simulation. A very rough escape criterion is set up, to decide that, definitely, an orbit starting close to a homographic solution has gone away from it. We found that orbits starting very close to some unstable homographic orbit can remain relatively close to them for very long time. Even if there is no linear stability one can consider that they have a kind of "practical" or "effective" stability. Furthermore, for the orbits displaying linear stability one can not prove, in general, the non-linear stability. Even if KAM theorem can be applied, in the case of three or more degrees of freedom there is no way to prevent from the existence of Arnol'd diffusion, but the possible escape is extremely slow. The idea is similar to what happens around totally elliptic fixed points, as studied in [2] for the Lagrangian solutions of the RTBP.

In the present case a reference orbit (a homographic one) can be unstable, but many invariant tori can be close, with sticky properties (as follows using standard tools of averaging) and, hence, the departure from the vicinity of them is a very slow process. This study is completed with a plot of the rate of escape.

As a final comment we consider the "essential" number of eigenvalues to be computed. In principle the system has 6 degrees of freedom and hence one has to consider 12 eigenvalues. Due to the energy (and time shift) we can skip two of them. As we can assume the components $\mathbf{c}_x$ and $\mathbf{c}_y$ equal to zero one can skip two additional eigenvalues. Finally the fact that $\mathbf{c}_z$ is constant and the node elimination allow to reduce to 6 essential eigenvalues. The reduction process can be seen like the one in the Euclidean problem, as described, e.g., in [8]. Anyway, for most of the analytical and numerical computations we shall not use reduction, but rather the non-relevant eigenvalues are skipped at the end of the computations. In this way the equations to integrate are kept easy and this is also used as an additional check.

2. **Stability of the relative equilibria.** The system (1) has a Lagrangian-like periodic solution in which the three bodies move on a parallel, forming an equilateral triangle for all time, and rotating with angular velocity ω. Let $r \in (0,1)$ be the radius of the parallel. Then the vertical coordinate $z = \pm\sqrt{1-r^2}$ remains constant. For concreteness we introduce the coordinates $\mathbf{q}_i = (x_i, y_i, z_i)^T$. Just asking that the values of z_i remain constant it is immediate to obtain $\omega = (24/(12r^2 - 9r^4)^{3/2})^{1/2}$.

It is clear that, when the radius tends to zero, the dynamics approaches the planar motion, but with present variables the value of ω in these periodic solutions tends to ∞. As a first step it is convenient to introduce scaled x, y variables and a new time τ defined as follows

$$x_i = rX_i, \quad y_i = rY_i, \quad t = r^{3/2}\tau. \tag{2}$$

In this way, when r tends to zero the equations tend to the planar ones plus a perturbation which is $\mathcal{O}(r^2)$. Let $'$ denote $d/d\tau$. Then the angular frequency becomes $\Omega = (24/(12 - 9r^2)^{3/2})^{1/2}$, bounded and bounded away from zero for the full range $r \in (0,1)$.

Next step is the introduction of a rotating frame. We define new variables ξ_i, η_i and the rotation $\mathcal{R}(\theta), \theta = \Omega\tau$, as

$$\begin{pmatrix} X_i \\ Y_i \end{pmatrix} = \mathcal{R} \begin{pmatrix} \xi_i \\ \eta_i \end{pmatrix}, \quad \mathcal{R}(\theta) = \begin{pmatrix} \cos(\theta) & -\sin(\theta) \\ \sin(\theta) & \cos(\theta) \end{pmatrix}. \tag{3}$$

The equations of motion become (the indices i, j ranging in $\{1,2,3\}$ and keeping in mind that r is a constant parameter here)

$$\begin{pmatrix} \xi_i'' \\ \eta_i'' \end{pmatrix} = \Omega^2 \begin{pmatrix} \xi_i \\ \eta_i \end{pmatrix} + 2\Omega \begin{pmatrix} \eta_i' \\ -\xi_i' \end{pmatrix} + \sum_{j\neq i} g_{i,j}^{-3/2} \left[\begin{pmatrix} \xi_j \\ \eta_j \end{pmatrix} - (\mathbf{q}_i, \mathbf{q}_j) \begin{pmatrix} \xi_i \\ \eta_i \end{pmatrix} \right] - r^2 h_i \begin{pmatrix} \xi_i \\ \eta_i \end{pmatrix}, \tag{4}$$

where

$$g_{i,j} = \rho_i^2 + \rho_j^2 - 2p_{i,j}\sqrt{z_{i,j}} - r^2(\rho_i^2\rho_j^2 + p_{i,j}^2), \quad \rho_i^2 = \xi_i^2 + \eta_i^2, \quad p_{i,j} = \xi_i\xi_j + \eta_i\eta_j,$$
$$z_{i,j} = (1 - r^2\rho_i^2)(1 - r^2\rho_j^2), \quad (\mathbf{q}_i, \mathbf{q}_j) = \sqrt{z_{i,j}} + r^2 p_{i,j},$$
$$h_i = \Omega^2\rho_i^2 + 2\Omega(\xi_i\eta_i' - \eta_i\xi_i') + (\xi_i')^2 + (\eta_i')^2 + r^2(\xi_i\xi_i' + \eta_i\eta_i')^2/(1 - r^2\rho_i^2).$$

Our present goal is to prove the following result.

Theorem 1. *Consider the Lagrangian-like periodic orbits of three equal masses moving on $\mathbb{S}^2$. Let the motion take place on a parallel with $|z| = \sqrt{1-r^2}$. Then the orbits are linearly stable (or totally elliptic) for $r \in (r_1, r_2) \cup (r_3, 1)$ and linearly unstable for $r \in (0, r_1) \cup (r_2, r_3)$. In the unstable domains the local behaviour around*

the orbits consists of two elliptic planes and a complex saddle. The bifurcations at $r_k, k = 1, 2, 3$ are Hamiltonian-Hopf bifurcations.

Remark 1. As it will be shown along the proof, the values of r_k at which the bifurcations are produced can be obtained from the zeros which belong to $(0, 1)$, of the polynomial

$$P_1(R) = 27R^5 + 3861R^4 - 11574R^3 + 11690R^2 - 4716R + 648,$$

where R denotes r^2. Approximate values are

$$r_1 = 0.55778526844099498188467226566148375,$$
$$r_2 = 0.68145469725865414807206661241888645,$$
$$r_3 = 0.92893280143637470996280353121615412.$$

Proof of Theorem 1.

It is easy to check that

$$\xi_1=1, \eta_1=0, \xi_2=-1/2, \eta_2=\sqrt{3}/2, \xi_3=\xi_2, \eta_3=-\eta_2, \xi_1'=\eta_1'=\xi_2'=\eta_2'=\xi_2'=\eta_2'=0 \tag{5}$$

is a fixed point in the rotating frame. We are interested on the eigenvalues of the differential of the vector field (4), written as a system of 12 first order equations, at that point.

The structure of the differential of the vector field at the fixed points is easily seen to be of the form

$$Df = \begin{pmatrix} 0 & I \\ A & B \end{pmatrix}.$$

Some tedious but elementary computations give

$$A = \Omega^2 \hat{A}$$

being $(24 - 18r^2)\hat{A}$ the matrix whose components $\hat{a}_{i,j}$ are given by

$\hat{a}_{1,1}=72r^4-120r^2+44$, $\hat{a}_{1,2}=\hat{a}_{2,1}=\hat{a}_{4,5}=\hat{a}_{6,3}=0$, $\hat{a}_{1,3}=\hat{a}_{1,5}=-18r^4+27r^2-10$,
$\hat{a}_{1,4}=-\hat{a}_{1,6}=(6r^4-11r^2+6)\sqrt{3}$, $\hat{a}_{2,2}=-24r^2+20$, $\hat{a}_{2,3}=-\hat{a}_{2,5}=(-9r^2+6)\sqrt{3}$,
$\hat{a}_{2,4}=\hat{a}_{2,6}=3r^2+2$, $\hat{a}_{3,1}=\hat{a}_{5,1}=-9r^4+24r^2-10$, $\hat{a}_{3,2}=-\hat{a}_{5,2}=(3r^4-10r^2+6)\sqrt{3}$,
$\hat{a}_{3,3}=\hat{a}_{5,5}=18r^4-48r^2+26$, $\hat{a}_{3,4}=\hat{a}_{4,3}=-\hat{a}_{5,6}=-\hat{a}_{6,5}=(-18r^4+24r^2-6)\sqrt{3}$,
$\hat{a}_{3,5}=\hat{a}_{5,3}=-6r^2+8$, $\hat{a}_{3,6}=-\hat{a}_{5,4}=(6r^4-2r^2)\sqrt{3}$, $\hat{a}_{4,1}=-\hat{a}_{6,1}=(9r^4-12r^2+6)\sqrt{3}$,
$\hat{a}_{4,2}=\hat{a}_{6,2}=-9r^4+6r^2+2$, $\hat{a}_{4,4}=\hat{a}_{6,6}=54r^4-96r^2+38$, $\hat{a}_{4,6}=\hat{a}_{6,4}=-18r^4+36r^2-16$,

and

$$B=\Omega\hat{B}, \quad \text{being} \quad \hat{B}=\begin{pmatrix} 0 & 2-2r^2 & 0 & 0 & 0 & 0 \\ -2 & 0 & 0 & 0 & 0 & 0 \\ 0 & 0 & -r^2\frac{\sqrt{3}}{2} & 2-\frac{r^2}{2} & 0 & 0 \\ 0 & 0 & -2+\frac{3r^2}{2} & r^2\frac{\sqrt{3}}{2} & 0 & 0 \\ 0 & 0 & 0 & 0 & r^2\frac{\sqrt{3}}{2} & 2-\frac{r^2}{2} \\ 0 & 0 & 0 & 0 & -2+\frac{3r^2}{2} & -r^2\frac{\sqrt{3}}{2} \end{pmatrix}.$$

We are interested in the characteristic multipliers of the periodic orbit, that is in $\lambda = \exp(\zeta T)$, where $T = 2\pi/\Omega$ is the period and ζ an eigenvalue of Df. Let us introduce μ such that $\zeta = \Omega\mu$ and then $\lambda = \exp(2\pi\mu)$. In this way we can skip the factor in Ω^2 in the characteristic polynomial, and the equation for μ becomes

$$p(\mu) := \det(\hat{A} + \mu\hat{B} - \mu^2 I) = 0.$$

Let now R denote r^2 and $M = \mu^2$. The characteristics polynomial, after multiplying by $(4-3R)^4$ to skip denominators, dividing by $M(M+1)$ to take out some eigenvalues associated to first integrals and removing a factor depending on R, nonzero in $[0,1]$, turns out to be

$$\begin{aligned} P(M) = \; & (27R^3 - 108R^2 + 144R - 64)M^4 \\ & +(81R^3 - 324R^2 + 432R - 192)M^3 \\ & +(-81R^5 + 810R^3 - 1608R^2 + 1212R - 336)M^2 \\ & +(54R^6 - 27R^5 - 900R^4 + 2788R^3 - 3376R^2 + 1812R - 352)M \\ & +(1350R^6 - 4050R^5 + 3780R^4 - 200R^3 - 1624R^2 + 888R - 144). \end{aligned}$$

We recall that the condition for the linear stability of the relative equilibria is that the solutions M of the previous equation be real and negative. In Figure 1 we plot the real zeros of $P(M)$ as a function of r. The values of r_1, r_2 and r_3 given in Remark 1, when the number of real negative zeros changes from 2 to 4 or vice versa are shown by short vertical lines.

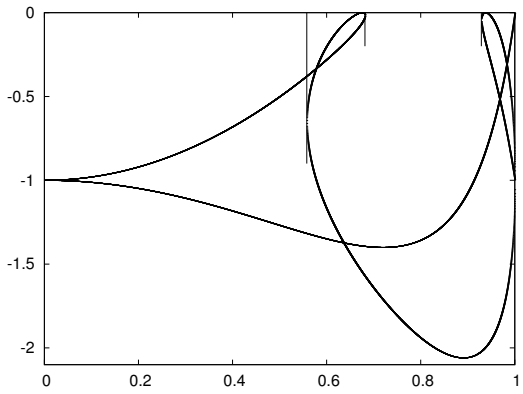

FIGURE 1. The evolution of the real zeros of $P(M)$ as a function of r.

We consider first the limit cases, $r = 0, 1$ ($R = 0, 1$) for $P(M)$. If $R = 0$ the roots are $M = -1$ (double) and $M = -1/2 \pm \sqrt{2}\,\mathrm{i}$. Last ones give $\mu = \pm 1/\sqrt{2} \pm \mathrm{i}$, the well known Siegel exponents for equal masses in the planar case, see [7]. If $R = 1$ the roots are $M = 0$ and $M = -1$ (triple). We have to consider first what happens for $R > 0$ small and for $R < 1$ but close to 1.

For R small the roots obtained by continuation of the Siegel exponents are simple and only move slightly. To analyze the behaviour of the other roots we set $M = -1 + N$. After simplification $P(M)$ becomes $10R^2 + 3RN - 4N^2 + \mathcal{O}(||(N,R)||^3)$ and a standard Newton polygon argument shows that the roots have expansions of the form $N = 2R + \mathcal{O}(R^2), N = -5R/4 + \mathcal{O}(R^2)$. Hence, M continues to be real and close to -1.

For R close to 1 we introduce $R = 1+S$ and expanding $P(M)$ around $S = 0, M = 0$ we obtain $-M+10S+\mathcal{O}(||(M,S)||^2)$. Hence the root $M = 0$ for $S = 0$ has the form $M = 10S + \mathcal{O}(S^2)$ and keeps being negative for $S < 0$ near zero. For the triple root we set $M = -1+N$ and then we obtain $144S^2+16NS+N^3+\mathcal{O}(S^3, S^2N, SN^2, N^4)$. Again a Newton polygon argument gives roots of the form $N = -9S + \mathcal{O}(S^2), N = \pm 4\sqrt{-S} + \mathcal{O}(S^{3/2})$. Therefore, for $S < 0$ near zero (i.e., $R < 1$) the roots M keep being real and close to -1.

Changes on the stability of the Lagrangian-like periodic orbits can be produced when a couple of conjugate imaginary roots μ become real (i.e., M crosses 0) or when two couples of conjugate imaginary roots collide and move outside the imaginary axis (i.e., M has a negative double root which moves to the complex), the so-called Hamiltonian-Hopf bifurcation.

Setting $M = 0$ in $P(M) = 0$ we find that the possible values for R are $R_{1,2} = (10 \pm \sqrt{10})/15$. These are double zeros, beyond the trivial zeros $R = 1, R = -2/3$. Let now write $R = R_{1,2} + S$. The expansions of $P(M)$ around $M = 0, S = 0$ give, in both cases (i.e., for $R = R_1$ and $R = R_2$), expressions of the form $\alpha M + \beta S^2 + \mathcal{O}(M^2, MS, S^3)$ with $\alpha < 0, \beta < 0$. Hence, the value of M is not crossing zero. This can be seen in Figure 1.

Finally it remains to check negative double roots for M. To this end we compute the resultant of $P(M)$ and $dP(M)/dM$ as a polynomial in R which factorizes as

$$R^2(R-1)^3(3R-4)^{10}(3R-1)^2 P_1(R) P_2(R)^2,$$

where P_1 and P_2 are irreducible polynomials of degree 5

$$P_1(R) = 27R^5 + 3861R^4 - 11574R^3 + 11690R^2 - 4716R + 648,$$

$$P_2(R) = 486R^5 - 2133R^4 + 4428R^3 - 4824R^2 + 2512R - 468.$$

The roots of the first three factors are irrelevant in the range of interest. The double factors $3R - 1, P_2(R)$ give rise to double zeros, but there are no complex roots for M because the roots return to the reals. This happens at values of R equal to $1/3$ and approximately equal to $0.4044168969, 0.9360332760, 0.9652070601$ (other zeros of P_2 being complex). But these concrete values are not relevant.

Hence, the only possible bifurcations are associated to the zeros of P_1. As $P_1(1) < 0, P_1(0) > 0$ one should have one root with $R > 1$ and another with $R < 0$. A simple computation gives three roots $R_1, R_2, R_3 \in (0, 1)$ which correspond to the radii r_1, r_2, r_3 given in Remark 1.

There are other values of r for which the corresponding values of μ are of the form $k\,\mathrm{i}/2, k \in \mathbb{Z}$ and, therefore, corresponding to eigenvalues of the monodromy matrix of the periodic orbit equal to ± 1. But these values of μ are simple and cannot give rise to bifurcations. This ends the proof of Theorem 1. □

The zeros of $P(M)$ as a function of $R = r^2$ have been computed numerically and from them the eigenvalues $\lambda_1, \ldots, \lambda_8$, being $\lambda_{j+4} = \lambda_j^{-1}$ for $j = 1, \ldots, 4$ are obtained. We recall that the eigenvalues already known to be associated to first integrals have been skipped. On the other hand we have computed all the characterictic multipliers by direct numerical integration of the equations (1). As expected four of them are equal to 1. For the remaining ones the results agree with the ones obtained from the roots of $P(M)$ within the expected numerical accuracy.

Moreover, as said at the Introduction, we can expect a further reduction. Indeed, it has been checked that the eigenvalues $\lambda_1, \ldots, \lambda_8$ are not independent, beyond the conditions imposed by the symplectic character. In any case, for the full range of $r \in (0, 1)$ one finds three indices j_1, j_2, j_3, the differences between them being always different from 4, such that $\lambda_{j_1}\lambda_{j_2}\lambda_{j_3} = 1$. This is the effect of the first integrals not taken into account until this point. It is immediate to check also that the same holds by taking the eigenvalues as $\exp(2\pi\mu_j)$ where $\mu_j^2 = M_j$ and M_j are the roots of the polynomial $P(M)$ for any value of $R \in [0, 1]$.

3. **Preliminaries for the homographic solutions.** Now we pass to the homographic orbits, keeping the constant curvature $\kappa = 1$ and scaling again time and momentum to normalise $m = 1$ for the three bodies.

We look for homographic solutions in the form

$$x_i = r(t)\cos(\theta(t)+(i-1)2\pi/3), \quad y_i = r(t)\sin(\theta(t)+(i-1)2\pi/3), \quad i = 1,2,3, \tag{6}$$

for some scalar functions $r(t), \theta(t)$. We recall that $\mathbf{q}_i = (x_i, y_i, z_i)$, $i = 1,2,3$. To study the homographic solutions we introduce $\mathbf{Q}_i = (x_i, y_i)$, $i = 1,2$ and a rotating and pulsating reference system as

$$\mathbf{Q}_i = r(t)\mathcal{R}(\theta(t))\mathbf{U}_i, \quad \mathbf{U}_i = (\xi_i, \eta_i)^T, \quad i = 1,2,3$$

where $\mathcal{R}(\theta)$ is the rotation defined in (3). We remark that if we take $r(t)$ as constant, and $\theta(t) = \Omega r^{-3/2} t$, we recover the change of variables introduced in Section 2. However, to study homographic solutions now, we preserve the initial time t.

The equations in the new variables become the following

$$\begin{aligned}\begin{pmatrix} \ddot{\xi}_i \\ \ddot{\eta}_i \end{pmatrix} &= \alpha_1 \begin{pmatrix} \dot{\xi}_i \\ \dot{\eta}_i \end{pmatrix} + \alpha_2 \begin{pmatrix} \dot{\eta}_i \\ -\dot{\xi}_i \end{pmatrix} + \alpha_3 \begin{pmatrix} \eta_i \\ -\xi_i \end{pmatrix} + \alpha_4 \begin{pmatrix} \xi_i \\ \eta_i \end{pmatrix} + \\ &+ \sum_{j=1,3,j\neq i} d_{i,j}^{-3/2} \left[\begin{pmatrix} \xi_j \\ \eta_j \end{pmatrix} - (\mathbf{q}_i, \mathbf{q}_j) \begin{pmatrix} \xi_i \\ \eta_i \end{pmatrix} \right] \end{aligned} \tag{7}$$

where

$$\alpha_1 = -2\frac{\dot{r}}{r}, \quad \alpha_2 = 2\dot{\theta}, \quad \alpha_3 = \frac{2\dot{r}\dot{\theta} + r\ddot{\theta}}{r}, \quad \alpha_4 = -\frac{(\ddot{r} - r\dot{\theta}^2)}{r} - (\dot{\mathbf{q}}_i, \dot{\mathbf{q}}_i), \quad d_{i,j} = 1 - (\mathbf{q}_i, \mathbf{q}_j)^2.$$

We are interested in the homographic solutions contained in northern hemisphere, so we can assume $z > 0$. Using the constrain $z_i^2 = 1 - r^2(\xi_i^2 + \eta_i^2)$, $i = 1,2,3$, the equations in (7) only depend on the variables ξ_i, η_i. A simple computation shows that

$$(\mathbf{q}_i, \mathbf{q}_j) = r^2(\xi_i\xi_j + \eta_i\eta_j) + \sqrt{(1 - r^2\rho_i^2)(1 - r^2\rho_j^2)}, \quad \rho_i^2 = \xi_i^2 + \eta_i^2,$$

$$\begin{aligned}(\dot{\mathbf{q}}_i, \dot{\mathbf{q}}_i) = (\dot{r}^2 + r^2\dot{\theta}^2)\rho_i^2 + 2r\dot{r}(\xi_i\dot{\xi}_i + \eta_i\dot{\eta}_i) + 2r^2\dot{\theta}(\xi_i\dot{\eta}_i - \eta_i\dot{\xi}_i) + r^2(\dot{\xi}_i^2 + \dot{\eta}_i^2) + \\ \frac{1}{1 - r^2\rho_i^2}\left[r\dot{r}\rho_i^2 + r^2(\xi_i\dot{\xi}_i + \eta_i\dot{\eta}_i)\right]^2\end{aligned}$$

It is easy to check that (5) is a fixed point of (7) if and only if $r(t)$, $\theta(t)$satisfy the following equations

$$\ddot{r} = \frac{c^2(1 - r^2)}{r^3} - \frac{r(\dot{r})^2}{1 - r^2} - \frac{24(1 - r^2)}{r^2(12 - 9r^2)^{3/2}}, \tag{8}$$

$$\dot{\theta} = c/r^2, \tag{9}$$

where c is the modulus of the angular momentum as before. We note that from (8) and (9) it follows that all the α_i coefficients in (7) only depend on $r(t), \dot{r}(t)$. In particular $\alpha_3 = 0$.

A fixed point of (8) is found at a given value of r when $c^2 = 3r(3 - 9r^2/4)^{-3/2}$ and then $\dot{\theta} = \omega$, as given before. Letting aside the values $r = 0$ and $r = 1$, for any c such that $c^2 \in (0, 8/\sqrt{3})$ there exists a unique fixed point $r = r_e$, $0 < r_e < 1$. This value of r corresponds to the relative equilibrium for that value of c. Note that close to $r = 0$ it is convenient to introduce scalings as done in Section 2 and that close to $r = 1$ the radius is a bad coordinate and we shall introduce later a more clear description using z as a good variable outside a neighborhood of the poles.

Let be $s = \dot{r}$ and multiply the system of first order equations by $h(r) = (1-r^2)^{-1}$. The equation (8) can be written as

$$\dot{r} = \frac{s}{1-r^2}, \quad \dot{s} = \frac{c^2}{r^3} - \frac{24}{r^2(12-9r^2)^{3/2}} - \frac{rs^2}{(1-r^2)^2},$$

which turns out to be Hamiltonian with Hamilton function

$$\mathcal{H}_r(r,s) = \frac{s^2}{2(1-r^2)} + \frac{c^2}{2r^2} + \frac{3r^2-2}{r(12-9r^2)^{1/2}}. \tag{10}$$

Given any c with $c^2 \in (0, 8/\sqrt{3})$ the phase portrait of the Hamiltonian (10) is qualitatively like the one plotted in Figure 2 left. There are periodic orbits surrounding the equilibrium point $(r,s) = (r_e, 0)$. We note that these periodic orbits give rise to homographic solutions. Each periodic orbit intersects the horizontal axis at two points with $r = r_1, r = r_2, r_1 < r_2$. Furthermore, there exists a lower limit value $r_{1,\lim}$ of r_1, which is found when we set $r_2 = 1$ and hence $r_{1,\lim}$ satisfies

$$c^2/(2r^2) + (3r^2-2)/(r(12-9r^2)^{1/2}) = c^2/2 + 1/\sqrt{3}.$$

It is clear that as r_1 increases towards r_e the value of r_2 decreases to r_e.

Note that from $r^2 + z^2 = 1$ follows $\dot{r} = -z\dot{z}/r$. Assume that an orbit tends linearly asymptotically to $z = 0$, say for $t \to +\infty$, that is, $\dot{z} = -mz + \mathcal{O}(z^2)$ for some positive m and let us write $r = 1 - \varepsilon$ for r close to 1. It follows immediately that, if $c < \sqrt{8/\sqrt{3}}$ then $\dot{r}$ has a dominant term in ε when $r \to 1$. However, if $\dot{z}$ tends to a finite value when $z \to 0$ and hence $r \to 1$, then the dominant term in $\dot{r}$ is of the order of $\varepsilon^{1/2}$. The point $(r, \dot{r}) = (1, 0)$ is degenerated. The degeneracy disappears in the $(z, \dot{z})$ variables, as it will be seen in (12).

The right part of Figure 2 displays the domain in (c, r) that will be used in Section 4 to study the stability of homographic solutions in the northern hemisphere. It is clear that for each one of the periodic orbits shown in the left part of the figure it is enough to take as initial point the minimum radius.

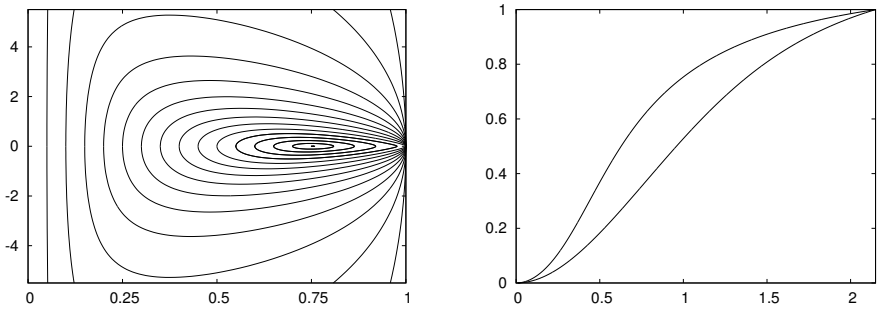

FIGURE 2. Left: Examples of homographic orbits in the $(r, \dot{r})$ variables around a relative equilibrium (near $r = 0.75$) for $c = 1$. Right: the relevant domain in the (c, r_1) variables: for each value of $c \in (0, (8/\sqrt{3})^{1/2})$ we display in the variable $r \in (0, 1)$ the range between $r_{1,\lim}$ and r_e that we shall use as initial data for homographic solutions.

To look for the Lagrangian-like solutions using z instead of r as variable we note that the equation equivalent to (8) using z is

$$\ddot{z} = -\frac{z}{1-z^2}(c^2 + (\dot{z})^2) + \frac{24z}{(1-z^2)^{1/2}(3+9z^2)^{3/2}}. \tag{11}$$

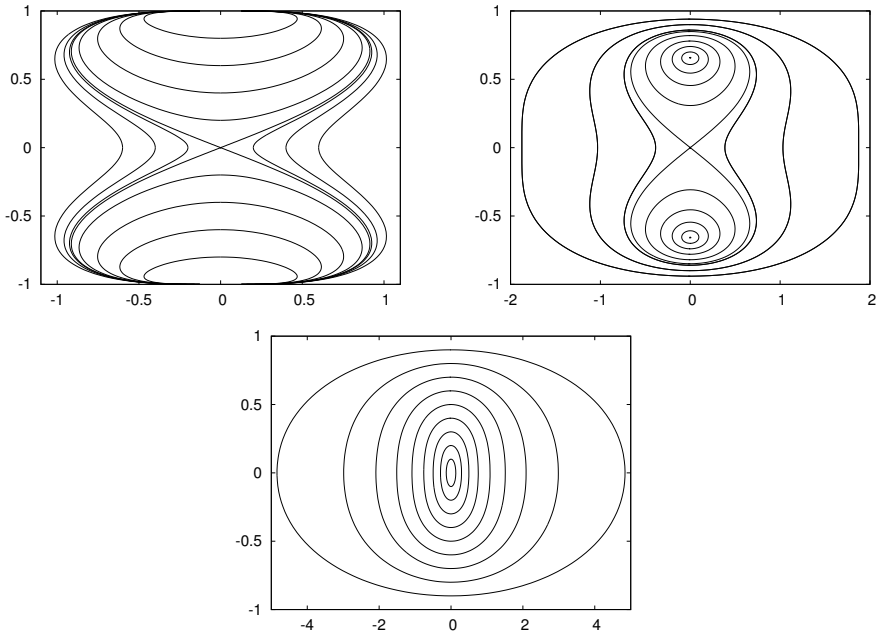

FIGURE 3. Examples of homographic orbits in the $(\dot{z}, z)$ variables, that can be read off as phase portrait of (12). Note that, to give a feeling of what happens on the sphere, the variable displayed in the vertical direction is z. The values of c are 0 (top left), 1 (top right) and 2.5 (bottom).

As in the previous case one can write (11) in Hamiltonian form, in that case without changing the time variable. Let us define $w = \dot{z}/(1-z^2)$ as variable canonically conjugated to z and then the new Hamiltonian is given by

$$\mathcal{H}_z(z,w) = \frac{w^2}{2}(1-z^2) + \frac{c^2}{2(1-z^2)} - \frac{3z^2-1}{[(1-z^2)(3+9z^2)]^{1/2}}. \tag{12}$$

Figure 3 shows the phase portrait for the values of c equal to 0, 1 and 2.5, last one greater than $(8/\sqrt{3})^{1/2}$. From these plots one can easily read off the description of the different types of Lagrangian-like solutions given at the Introduction.

Our next goal is to study the stability of the homographic orbits.

4. **Stability of the homographic solutions.** The stability of the homographic solutions reduces to the analysis of a fixed point in a non-autonomous periodically depending system as given by (7). Both equations (8) and (9) give r and θ as functions of t with $r(t)$ periodic. Note that in one period the angle turned by θ is not a multiple of 2π in general. Then the homographic solution (6) is no longer periodic but quasiperiodic in a fixed frame. An example of the motion of the first mass in one of these orbits is shown in Figure 4.

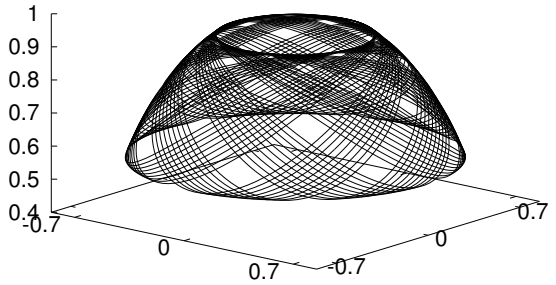

FIGURE 4. Part of an homographic solution, displaying $(x_1(t), y_1(t), z_1(t))$ in a fixed frame. The other bodies have the (x, y) coordinates rotated by $2\pi/3$ and $4\pi/3$, respectively. These orbits are quasiperiodic, in general. The orbit displayed here has been computed for $c = 0.7$ and initial values for (r, θ) equal to $(0.39, 0)$.

To face the stability problem we have used numerical methods. Using (7) we have computed numerically the monodromy matrix associated to the fixed point (5) for a grid of values in (c, r_1). From this matrix we have computed the traces which allow to obtain the eigenvalues, as it will be explained later.

Alternatively, for a given value of c, the equations of motion (1) are integrated with initial conditions given by (6) being $(r(t), \theta(t))$ solutions of the equations (8) and (9), starting at t=0 with a value of $r(0)$ in the range $(r_{1,\lim}, r_e]$ and $\dot{r}(0) = \theta(0) = 0$. Let us define $\mathcal{R}$ as $\sum_{j=1}^{3}(x_j^2 + y_j^2)$. It is obvious that $\dot{\mathcal{R}} = \sum_{j=1}^{3}(x_j\dot{x_j} + y_j\dot{y_j})$ is zero at $t = 0$. In fact $\mathcal{R}$ has a minimum there and then $\ddot{\mathcal{R}} > 0$ for the homographic orbits which are not relative equilibria, according to the choice of $r(0)$. We shall use $\dot{\mathcal{R}} = 0$ at a minimum of $\mathcal{R}$ as Poincaré section, Σ, on a fixed level of energy $H = h$ corresponding to the homographic solutions. We use in Σ the local variables $(y_1, x_2, y_2, x_3, y_3, \dot{y_1}, \dot{x_2}, \dot{y_2}, \dot{x_3}, \dot{y_3})$ and $x_1, \dot{x_1}$ are recovered from $\dot{\mathcal{R}} = 0,\ H = h$.

Then the Poincaré map $\mathcal{P}$ with respect to Σ and its differential $D\mathcal{P}$ can be computed by integration of (1) and the first variational equations. We remark that $\mathcal{P}$ has an extra rotation due to the fact that the final value θ_f of θ is not a multiple of 2π. It is easy to "correct" this irrelevant fact by applying a rotation of angle $-\theta_f$ to $\mathcal{P}$ and $D\mathcal{P}$. In that way the final point under $\mathcal{P}$ coincides with the initial one (except by the effect of tiny numerical errors). Another point worth to be commented is that the local variables used in Σ are not canonically conjugated. Hence $D\mathcal{P}$ is not a symplectic matrix, but it is conjugated to the symplectic matrix that one would obtain by doing first a change to positions and conjugated momenta in the equations in (1).

Hence one has to look for the eigenvalues of $D\mathcal{P}$. It is immediately realized that two of them are equal to 1, associated to the fact that the components $\mathbf{c}_x$ and $\mathbf{c}_y$ of $\mathbf{c}$ are first integrals. The characteristic polynomial of $D\mathcal{P}$ is of the form

$$P_{10}(\lambda) = (\lambda - 1)^2(\lambda^8 + 1 + a_1(\lambda^7 + \lambda) + a_2(\lambda^6 + \lambda^2) + a_3(\lambda^5 + \lambda^3) + a_4\lambda^4) \quad (13)$$

and the values of a_1, a_2, a_3, a_4 are computed from the entries of $D\mathcal{P}$. Instead of computing the eigenvalues $\lambda_j, j = 1, \ldots, 8$ with $\lambda_j\lambda_{j+4} = 1$ for $j = 1, 2, 3, 4$ as solutions of (13) it is simpler to compute the associated traces $\mathrm{Tr}_j = \lambda_j + \lambda_{j+4}$. The

corresponding equation is

$$\mathrm{Tr}^4 + c_1\mathrm{Tr}^3 + c_2\mathrm{Tr}^2 + c_3\mathrm{Tr} + c_4 = 0, \tag{14}$$

where

$$c_1 = a_1, \quad c_2 = a_2 - 4, \quad c_3 = a_3 - 3a_1, \quad c_4 = a_4 - 2a_2 + 2.$$

The linear stability condition is that all the zeros of (14) be real and range in the interval $(-2, 2)$.

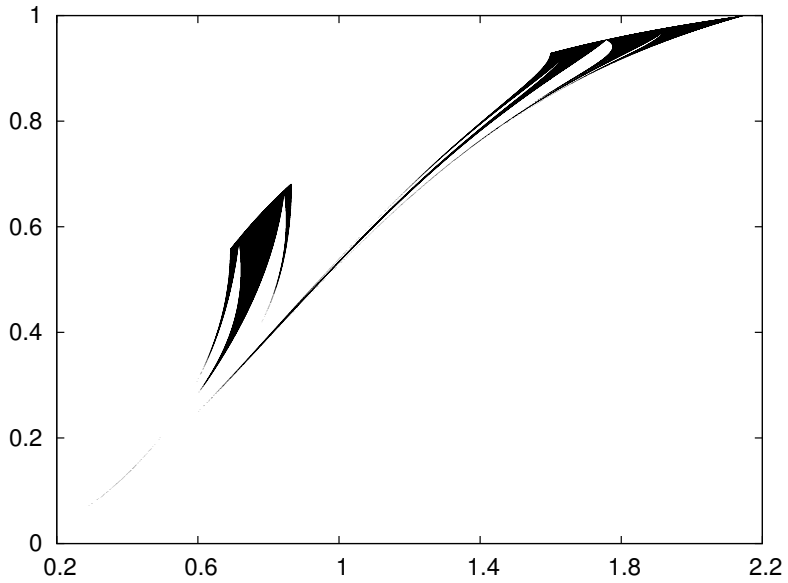

FIGURE 5. The set of values in the (c, r) variables, with $r \le r_e(c)$ for which the homographic solutions are found to be linearly stable.

The methods described have been applied to values of c, r in the domain shown on the right side of Figure 2 with steps in c and r equal to $\Delta c = \Delta r = 5 \times 10^5$. In all near $N_0 = 104.9 \times 10^6$ cases have been examined. A relatively small, but still important fraction of them, near 14.05×10^6 show linear stability. The results of both methods coincide and are displayed in Figure 5. As it should be, the part of the domain which is linearly stable and has the relative equilibrium solutions as boundary, coincides with the result given by Theorem 1. It is also worth to mention the following facts:

(i) Similar to what happens in the case of relative equilibria, there are two "superfluous" eigenvalues related to additional first integrals not taken into account: the invariance of $\mathbf{c}_z$ and the node elimination. It is checked that, in all cases and within the accuracy of the numerical computations, there exist indices j_1, j_2, j_3, j_4, not two of them differing in 4 units, such that $\lambda_{j_1}\lambda_{j_2}\lambda_{j_3}\lambda_{j_4} = 1$.

(ii) The lose of stability observed at the boundaries of the set shown in Figure 5, different from the values $r_{1,\mathrm{lim}}(c), r_e(c)$, seems to be due to Hamiltonian-Hopf bifurcationsi in all cases.

(iii) In the figure one can observe tiny filaments of stability close to the boundary associated to $r_{1,\mathrm{lim}}(c)$. In analogy to what happens in the general planar 3-body problem (see [6]) one can conjecture the role played by the separatrix

which appears in Figure 2, an orbit tending asymptotically to $r = 1$ ($z = 0$) for $t \to \pm\infty$, more clearly seen in Figure 3 top right. Using a standard argument one can blow up the degenerate point $(r, \dot{r}) = (1, 0)$ into a full line with two fixed hyperbolic points having an heteroclinic connection between them. The separatrix is seen as another heteroclinic connection between these points. The analysis of the vicinity of these connections allows to prove the existence of stability transitions. See [6] for details.

5. **Global aspects around the homographic solutions.** In order to see which is the role of linear stability/instability in the dynamics of the orbits close to homographic ones, a massive simulation by long time direct numerical integration has been carried out. Concretely, this has been done for each one of the $\approx 104.9 \times 10^6$ initial conditions considered in Section 4. Even starting at the theoretical values of a homographic orbit, the numerical errors move the solution to a vicinity of it and can reveal the (nonlinear) "effective" stability or the instability. We shall consider all these initial conditions as pixels in a plot.

The method used for the simulation proceeds as follows:

1) Start the integration for each pixel using initial data as explained in Section 4.
2) Define an "escape set" in a somewhat arbitrary way, just to detect that the solution has moved away from the homographic orbit. In the simulations we decide that a solution escapes if one of the following quantities is below 10^{-3}:
   i) $r_i = (x_i^2 + y_i^2)^{1/2}, i = 1, 2, 3,$
   ii) $z_i, i = 1, 2, 3,$
   iii) the distance between two of the bodies.
3) The integration is stopped when either a escape is produced or a maximal time t_{f_1} is reached. The set of pixels which subsist at that time is denoted as $\mathcal{S}_1$.
4) At that point a new maximal time $t_{f_2} > t_{f_1}$ is used but only some pixels are checked. As points which are deeply inside $\mathcal{S}_1$ can be expected to be more stable that the ones close to the boundary, we define a "deepness" parameter d_2. Every pixel in $\mathcal{S}_1$, say of indices j, k so that $c = j\Delta c$, $r = k\Delta r$, such that another pixel of indices j', k' with $|j - j'| \le d_2, |k - k'| \le d_2$ has escaped, is checked up to the time t_{f_2} and discarded if it escapes in turn. The process is repeated until all the current points of deepness d_2 subsist until $t = t_{f_2}$. The set of pixels which remain is denoted as $\mathcal{S}_2$.
5) The previous process is repeated starting with $\mathcal{S}_2$ with new values of the final time and the deepness: $t_{f_3} > t_{f_2}$ and $d_3 > d_2$. And then the checks are stopped with a new, smallest, set of pixels $\mathcal{S}_3$.

The concrete values used for t_{f_1}, t_{f_2} and t_{f_3} are $10^4, 10^5$ and 10^6 and for d_2, d_3 the values 3 and 5 have been adopted.

The results, as it can be expected, show that all the pixels which belong to the set shown in Figure 5 belong to the non-escaping set $\mathcal{S}_3$. Diffusion can occur but it is extremely slow. But the set $\mathcal{S}_3$ contains more points. Some selected regions on the (c, r)-plane are shown in Figure 6. The gray regions correspond to points in the domain of linear stability of Figure 5 and the black dots are pixels which correspond to homographic solutions which are linearly unstable, but they do not "escape" up to $t = t_{f_3} = 10^6$.

We note that in these enlarged plots one can distinguish several tiny domains of linear instability, specially close to $r_{1,\lim}(c)$, but an important part of them is non-escaping until $t = t_{f_3}$. These tiny domains seem to reach the relative equilibria, as it

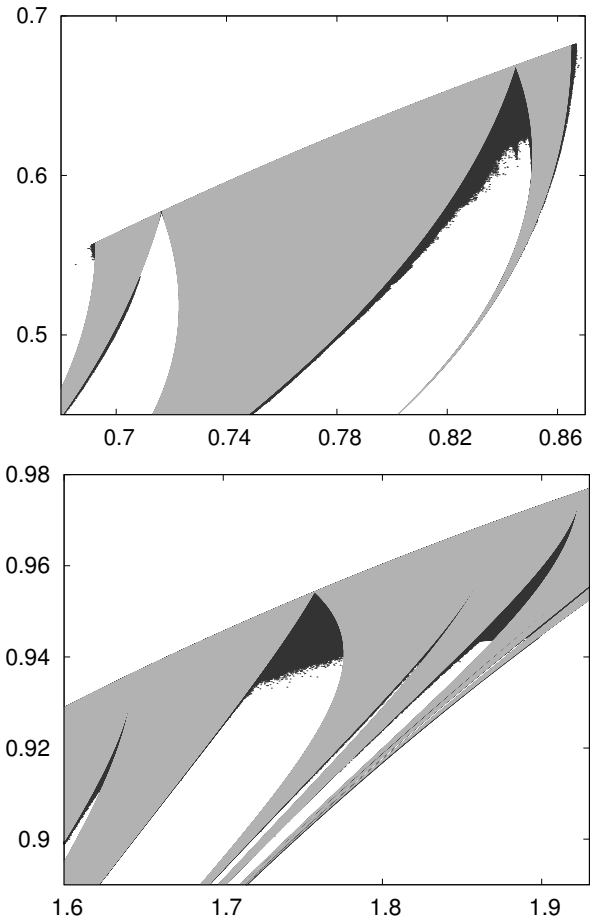

FIGURE 6. Two selected domains in the (c, r)-plane for which an abundant set of non-escaping points (in black) outside the domain of linear stability (in gray) has been found.

has been checked for some of the largest ones, but they are extremely tiny and quite soon they are below the pixel resolution. Most of them are almost irrelevant from a measure point of view. The explanation of its non-escaping character is rather simple. Points which start at a linearly unstable homographic solution will go away because of the numerical errors in the initial data and the ones which appear in the integration of the ODE. These errors produce some component along the unstable direction(s) and this component increases with time. But there can be plenty of nearby invariant tori. The orbit can come close to them and became "effectively stable" for a long time. An example is shown in Figure 7. On it we represent iterates of the Poincaré map $\mathcal{P}$, associated to the section $\dot{\mathcal{R}} = 0$ introduced in Section 4, for two sets of initial data. One of them has parameters $(c, r) = (0.84, 0.65)$ and belongs to the stable (gray) set in Figure 6 top. The other has $(c, r) = (0.84, 0.62)$ and belongs to the unstable (black) set in the same plot. Up to 10^6 iterates of $\mathcal{P}$ have been computed in both cases, but only one every 100 iterates is displayed. The time span in both cases is $\approx 2.8 \times 10^6$ units. In the plot the variables shown

are the values of (x_1, x_2, x_3), the points in black corresponding to $r = 0.65$ and the ones in gray to $r = 0.62$. Despite the maximal Lyapunov exponent for the last case is $\Lambda \approx 0.053785$ the orbit seems to be confined, not far from the stable one, for a very long time.

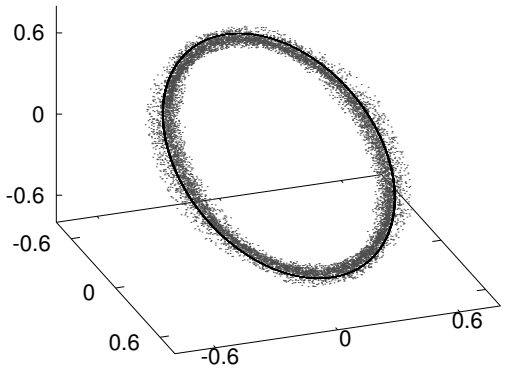

FIGURE 7. Poincaré iterates in $\dot{\mathcal{R}} = 0$ for a homographic stable orbit (in black) and for a nearby unstable one (in gray) which is not escaping for a long time. See the text for details.

As a final point we comment on the "rate of escape" observed in the previous simulations. When we start the iterations with N_0 pixels, most of them (near 80%) escape quickly, before $t = 100$. Then a slower rate of escape is seen, so that at $t = 10^4$ the number of non-escaped pixels is $\approx 15.6 \times 10^6$. This reduces to $\approx 15.0 \times 10^6$ for $t = 10^6$, still far away of the number of pixels ($\approx 14.05 \times 10^6$) associated to linear stability. Figure 8 shows the rate of decay. It is quite slow, giving an evidence of the strong sticky character of invariant tori which exist close to the some unstable homographic solutions.

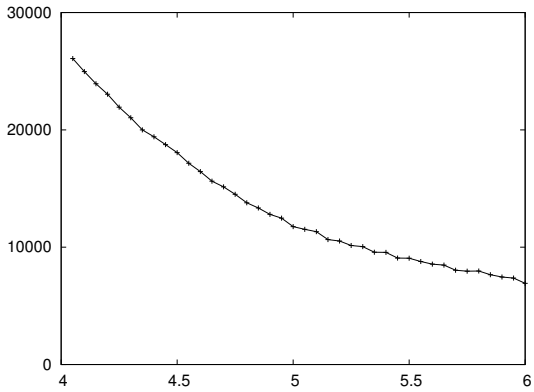

FIGURE 8. Using $\log_{10}$ scale for the time between 10^4 and 10^6 and 40 divisions in that scale (1 division amount to multiply t by 1.122) for every value $t_j = 10^{4+j/20}$ we display the number of points which escape between t_{j-1} and t_j.

6. **Future work.** In a natural way there are several possible extensions of the present work. Just to mention a few one can consider

1) To extend the linear stability analysis to other values of the curvature κ. For instance, how the curvature influences the fraction of linearly stable relative equilibria?
2) To carry out an analysis of the vicinity of the separatrix orbits shown in Figure 3 top right and bottom.
3) To do a massive check of the applicability of KAM theorem around the linearly stable solutions, using the standard jet transport methods (see, e.g., [3]) and to validate rigorously a sample of them.
4) To derive a theoretical approach, applicable to many other problems, which allows to explain the rates of escape obtained in Section 5.

Acknowledgements. The authors are deeply indebted to Florin Diacu and Ernesto Peérez-Chavela for suggesting the study of this problem and the interest shown in the development of the work. The research of both authors has been supported by grants MTM2006-05849/Consolider (Spain) and 2009 SGR 67 (Catalonia). The computing facilities of the Dynamical Systems Group of the Universitat de Barcelona have been largely used.

REFERENCES

[1] F. Diacu and E. Pérez-Chavela, "Homographic solutions of the curved 3-body problem," Journal of Differential Equations, **250** (2011), 340–366.
[2] A. Giorgilli, A. Delshams, E. Fontich, L. Galgani and C. Simó, "Effective stability for a Hamiltonian system near an elliptic equilibrium point, with an application to the restricted three body problem," Journal of Differential Equations, **77** (1989), 167–198.
[3] T. Kapela and C. Simó, "Rigorous KAM results around arbitrary periodic orbits for Hamiltonian Systems" Submitted for publication, 2011.
[4] R. Martínez, A. Samà and C. Simó, "Stability of homographic solutions of the planar three-body problem with homogeneous potentials", Proceedings Equadiff03, F. Dumortier et al. editors, 1005–1010, World Scientific, 2005.
[5] R. Martínez, A. Samà and C. Simó, "Stability diagram for 4D linear periodic systems with applications to homographic solutions," Journal of Differential Equations, **226** (2006), 619–651.
[6] R. Martínez, A. Samà and C. Simó, "Analysis of the stability of a family of singular–limit linear periodic systems in R^4. Applications," Journal of Differential Equations, **226** (2006), 652–686.
[7] C. Siegel and J. Moser, Lectures on Celestial Mechanics, Springer, 1971.
[8] E. T. Whittaker, A treatise on the Analytical Dynamics of Particles and Rigid Bodies, Cambridge Univ. Press, fourth edition, reprinted, 1970.

Received

E-mail address: reginamb@mat.uab.cat
E-mail address: carles@maia.ub.es